RSC Advances

ROYAL SOCIETY OF CHEMISTRY

www.rsc.org/advances

Assembly of MnO_2 nanowires@reduced graphene oxide hybrid with interconnected structure for high performance lithium ion battery

Zhangpeng Li[ab], Jinqing Wang*[a], Zhaofeng Wang[a], Yongbing Tang[b], Chun-Sing Lee*[b], Shengrong Yang[a]

[a] State Key Laboratory of Solid Lubrication, Lanzhou Institute of Chemical Physics, Chinese Academy of Sciences, Lanzhou 730000, P. R. China

[b] Center of Super-Diamond and Advanced Films (COSDAF), Department of Physics and Materials Science, City University of Hong Kong, Kowloon, Hong Kong SAR, P. R. China

Corresponding authors. Tel.: +86-931-4968076 (J. Wang); +852-34427826 (C. Lee)

E-mail addresses: jqwang@licp.cas.cn (J. Wang); apcslee@cityu.edu.hk (C. Lee)

Abstract

A facile strategy is developed to fabricate a MnO_2 nanowires/reduced graphene oxide (rGO) hybrid with an interconnected structure. Morphology and microstructure of the hybrid is examined by field emission scanning electron microscopy, transmission electron microscopy, and X-ray diffraction analysis. The electrochemical properties of MnO_2 nanowire as an anode material for lithium-ion batteries is improved by this general strategy involving the addition of the rGO sheets to the nanowires, producing MnO_2 nanowires@rGO hybrid (MGH). The rGO effectively buffers the volume changes during lithiation/delithiation process, allowing the hybrid to retain its structure, without sacrificing its electrochemical performance. As a result, MGH delivers a high reversible capacity of 1079 mAh g^{-1} over 200 cycles at a current density of 500 mA g^{-1}, and excellent rate capability, thus such a quite stable hybrid exhibits great potential as an anode material for lithium ion batteries.

Keywords: Interconnected; Graphene; MnO_2; Anode; Lithium ion battery

1. Introduction

Lithium ion batteries (LIBs) have been widely used in portable electronics, electrical vehicles and renewable energy source since they were successfully commercialized by Sony [1-3]. With the growing need for higher capacity and improved cycle characteristics, numerous attempts have been made to develop new electrode materials for next-generation LIBs. For anode materials, transition metal oxides are promising candidates for LIBs largely due to their higher theoretical capacity than commercial graphite anode [4-7]. Among them, MnO_2 is considered as a good candidate because of its low conversion potential, high theoretical capacity (1233 mAh g^{-1}, about 3.5 times that of commonly used graphite anode), low cost, and nontoxic nature [8-10]. However, it suffers from poor cycling stability and rate capability due to its severe volume change during charge/discharge process and poor electronic conductivity (10^{-5}-10^{-6} S cm^{-1}) [8, 11], which are critical barriers to their practical utilization. Up to date, it still remains a great challenge to fabricate a stable MnO_2 anode over extended cycling with high reversible capacity and excellent rate capability.

To resolve the problems mentioned above, various strategies have been developed and a number of research progresses have been achieved in the past several years, such as constructing MnO_2 nanostructures and fabricating MnO_2/carbon hybrids [12, 13]. Using nanostructured MnO_2 with rational design and fabrication is a popular path to improve its electrochemical performance [11]. Among them, MnO_2 nanowires represent a unique candidate with several exciting advantages. Firstly, the high

surface-to-volume ratios of nanowires allow for fast penetration of electrolyte solution into a deep portion of nanowires, as well as rapid electrochemical reactions over the surface. Secondly, a high lithium ion flux can be achieved by the large surface area compared with their bulk counterpart. More importantly, owning to the extremely short distance for lithium ions transportation within the nanowires, the rate capability can be significantly enhanced. On the other hand, carbon coating is an effective strategy to tackle the poor conductivity issue. Furthermore, the carbon can also act as a mechanical buffer to release strain during cycling and to enhance lithium diffusion into the electrode [14-16]. Among the carbon materials, graphene has attracted much interest for energy-storage applications because of its superior electrical conductivity, chemical tolerance and broad electrochemical window [17-20]. A lot of attempts have been made to improve the lithium storage performance by introducing graphene component, such as graphene/SnO_2, [21, 22] graphene/Co_3O_4, [7, 23] graphene/FeO_x, [24, 25] and graphene/MnO_x, [26] et al.

Recently, it has been demonstrated that the rGO sheets can be assembled onto the surface of positive charged nanostructures, such as nanoparticles [27-29] and nanofibers [30, 31]. Inspired by this, herein, a facile electrostatic adsorption method was employed to fabricate MnO_2 nanowires@rGO hybrid (MGH). Briefly, MnO_2 nanowires were firstly treated with poly(diallyldimethylammonium chloride) (PDDA) to form a positive charged surface and then negative rGO sheets were introduced to join the MnO_2 nanowires and the rGO sheets together. The strong electrostatic adsorption and the 2D morphology of the rGO sheets render the hybrid material an

improved electrochemical performance. A high reversible capacity of 1079 mAh g^{-1} over 200 cycles at a current density of 500 mA g^{-1} and capacity of 272 mAh g^{-1} at a current density of 10000 mA g^{-1} can be obtained. Most importantly, such a facile electrostatic adsorption method is potentially extendable to many other LIB materials.

2. Experimental

Fabrication of MGH: MnO_2 nanowires were prepared by hydrothermal method according to a previous report [32]. To fabricate MGH, MnO_2 nanowires (0.1 g) were first dispersed in 100 mL 1 wt.% PDDA (Mw = 400 000-500 000) by sonication for 20 min, then the modified MnO_2 nanowires were separated by centrifugation and rinsed by deionized water, then the positively charged MnO_2 nanowires were added into 100 mL rGO solution (0. 125 mg mL^{-1}) and additionally aged for 30 min. Finally, the precipitate was collected by centrifugation and washed with deionized water, and then freeze-dried overnight.

Characterization: Morphologies and structures of the as-prepared samples were investigated with field-emission scanning electron microscopy (FESEM, JEOL JSM-6701F), transmission electron microscopy and selected area electron diffraction (TEM, FEI Tecnai G^2 F30), atomic force microscopy (AFM, VEECO Nanoscope IIIa), and X-ray diffraction instrument (XRD, Philips X'pert Pro MPD using Cu-Kα radiation and graphite monochrometer, λ = 0.154056 nm).

Electrochemical Measurements: Electrochemical characterizations were measured with CR2032 coin-type test cells assembled in a dry argon-filled glove box (MBRAUN, MB 200B) with an oxygen concentration below 1 ppm. The working

electrodes were prepared by mixing the composite, carbon black, and carboxyl methyl cellulose (CMC) at a weight ratio of 70:20:10 and pasted onto a copper foil. The copper foil was cut into disk electrodes (14 mm in diameter) and the mass-loading density was 1.02 ± 0.16 mg cm^{-2}. The test cell consists of a working electrode and a lithium counter electrode, which were separated by Celgard 2400 (Celgard, Inc., USA). The electrolyte is a solution of 1 M $LiPF_6$ in ethylene carbonate (EC)/dimethyl carbonate (DMC) (1:1 in volume). Galvanostatic discharge/charge experiments were carried out with a MACCOR 4000 battery test system over a voltage window of 0.01-3.0 V (vs. Li^+/Li). Cycle voltammetry was measured with a CHI 660D electrochemical workstation. Electrochemical impedance spectroscopy (EIS) measurements were performed using ZAHNER-elektrik IM6 impedance measurement unit over a frequency range of 0.01-10^5 Hz with an AC amplitude of 5 mV.

3. Results and Discussion

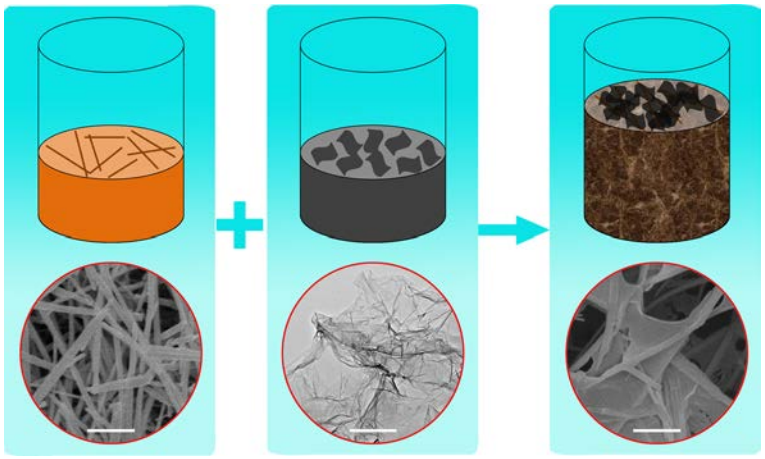

Scheme 1 Fabrication process of MGH.

Scheme 1 illustrates the fabrication process of the MGH. The MnO_2 nanowires were firstly immersed in PDDA solution to render the surface of nanowires positive charged. Whereas, rGO sheets present negative charge originating from the ionization

of the carboxylic acid and phenolic hydroxyl groups on their surface [33]. Adding the positively charged MnO_2 nanowires into the rGO dispersion can direct the uniform wrapping of rGO sheets on the surface of MnO_2 nanowires by the electrostatic interaction attraction.

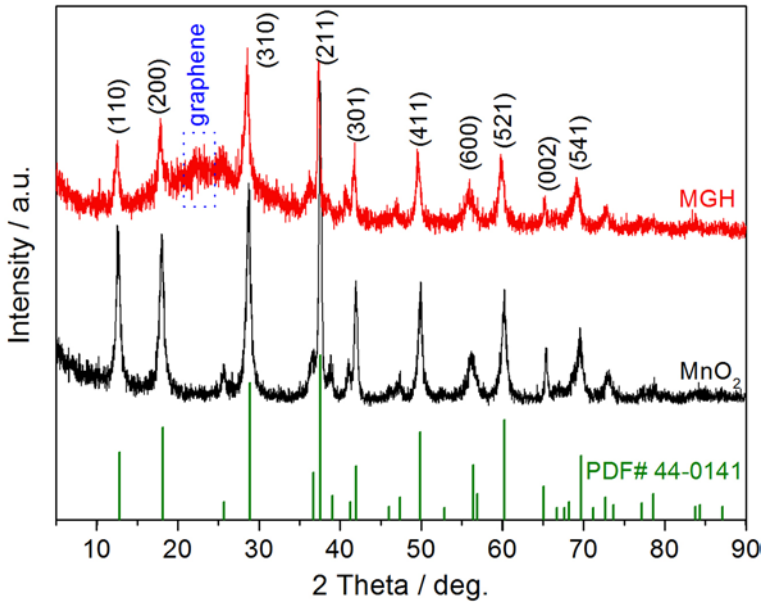

Fig. 1 XRD patterns of MnO_2 and MGH.

XRD patterns of the MnO_2 nanowires and MGH are shown in Fig. 1. The XRD pattern of the MnO_2 nanowires can be indexed to the tetragonal phase α-MnO_2 (JCPDS: 44-0141). Compared with the pattern of MnO_2 nanowire, an additional broad peak at around $2\theta = 23^{o}$ corresponds to the (002) planes of carbon materials can be observed, suggesting the existence of rGO in the hybrid. In order to determine the amount of MnO_2 in the hybrid, thermogravimetric (TG) analysis was performed. From TG curve of the hybrid (Fig. S1 in *Supporting Information*), the amount of MnO_2 in the hybrid is estimated to be about 85 wt.%.

Morphologies of the as-prepared samples were characterized by AFM, FESEM and TEM. Fig. 2a is an AFM morphological image and a corresponding cross-section

analysis of the as-prepared rGO on a silicon substrate. The average thickness of rGO sheets is approximately 0.9 nm, which is in good agreement with the reported value of this parameter in the literature [34], indicating that a single-layered rGO sheet has been obtained. FESEM images in Fig. 2b give the general morphology of the MnO_2 nanowires. It can be seen that the nanowires have length of several micrometers and tens of nanometers in diameter. After rGO wrapping, it can be noted that most of the MnO_2 nanowires were covered with rGO (Fig. 2c), indicating an efficient wrapping process. Furthermore, the rGO sheets not only uniformly wrap around the MnO_2 nanowires, but also connect the MnO_2 nanowires forming a homogeneous net-like architecture.

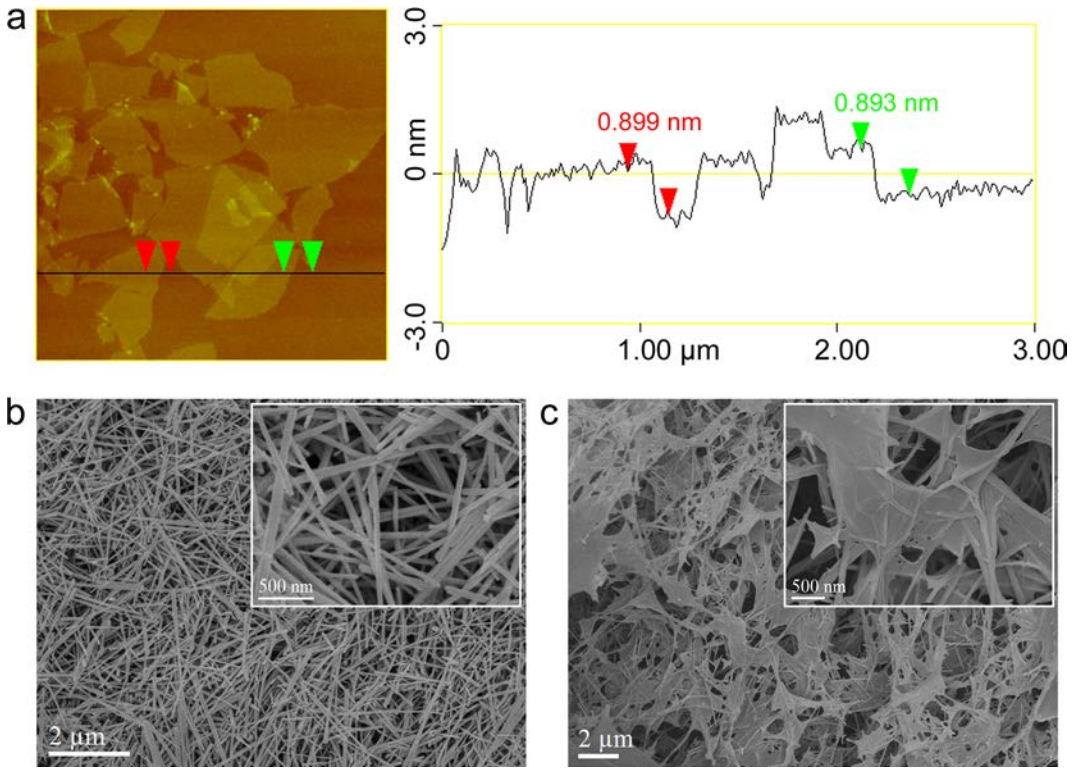

Fig. 2 (a) AFM morphological image and a corresponding cross-section analysis of the as-prepared rGO; b, c) FESEM images of MnO_2 nanowires and MGH.

TEM images of the MGH are shown in Fig. 3. As shown in Figs. 3a and b, the successfully wrapped of the MnO_2 nanowires by the rGO sheets can be clearly seen. Fig. 3c shows a high-resolution TEM image of the hybrid, further revealing that the MnO_2 nanowires are tightly wrapped by rGO. The lattice fringes give an interplanar spacing of 0.24 nm, corresponding to that of the (211) lattice planes of α-MnO_2 crystal. The unique architecture not only prevent the directly exposure of MnO_2 nanowire to the electrolyte, but also facilitate electron transfer.

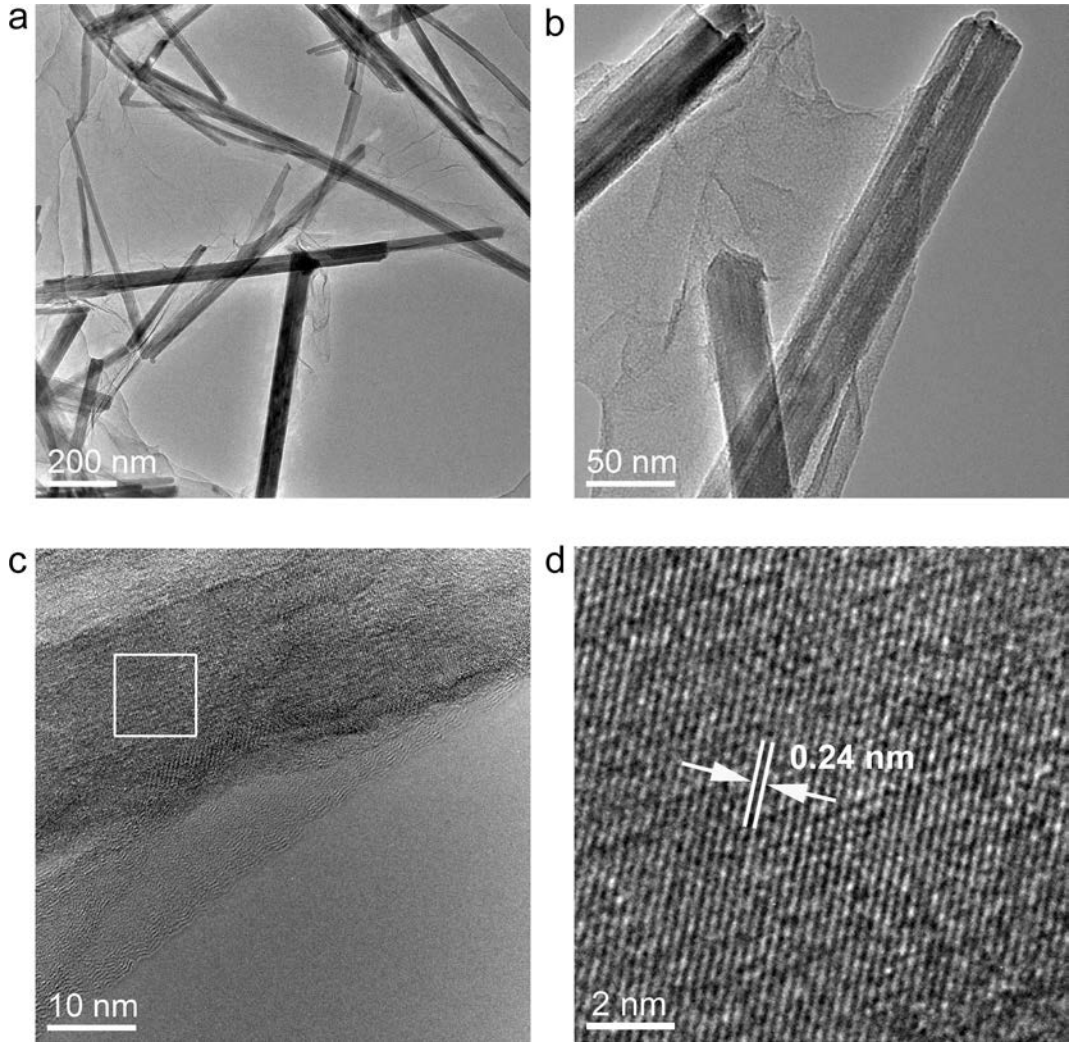

Fig. 3 (a, b) TEM and (c, d) HRTEM images of the MGH. Fig. d is the enlarged HRTEM image of the outlined area in Fig. c.

To explore the electrochemical properties of the as-prepared MGH, cycle

voltammetry (CV) and discharge/charge tests were performed. Fig. 4a shows the typical CV curves for the prepared MGH anode in the voltage window of 0.01-3.0 V (vs. Li^+/Li) at a scan rate of 0.1 mV s^{-1}. As shown in Fig. 4a, a broad and weak cathodic peak at about 0.7 V and a sharp peak at 0.1 V in the first cycle. The former can be assigned to the reduction of Mn^{4+} to Mn^{2+}, the latter is associated with the reduction of Mn^{2+} to Mn^0 and the formation of a solid electrolyte interface (SEI) layer with a reversible polymer/gel like film at the interface of electrolyte and electrode [35-38]. In the subsequent cycles, the cathodic peak at 0.7 V disappears and the sharp cathodic peak at the low potential region shifts to 0.2 V, which is attributed to structural or textural changes due to the formation of Li_2O and metallic manganese [36]. Two peaks located at 1.2 and 2.1 V are observed at the anodic process, which could be ascribed to the oxidation of Mn^0 to Mn^{4+} and the decomposition of the polymer/gel layer, respectively. The well overlapped peaks indicate a good electrochemical reversiblility and structural stability for the hybrid during the lithiation/delithiation processes from the second cycle onwards [39].

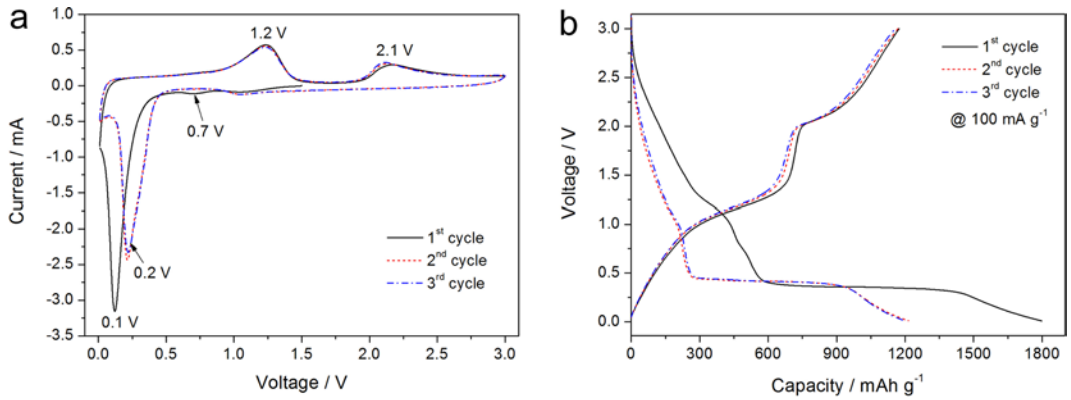

Fig. 4 (a) CV curves of the MGH at a scan rate of 0.1 mV s^{-1}; (b) Discharge and charge voltage profiles of the MGH at a current density of 100 mA g^{-1}.

Fig. 4b shows the first three discharge-charge profiles of the hybrid at a current density of 100 mA g^{-1}. It can be seen that there are notable discharge and charge voltage plateaus from the discharge-charge curves. The voltage plateau in the range of 0.32-0.45 V versus Li^+/Li for lithiation process and 1.0-2.2 V for delithiation process are in good accordance with those of MnO_2 reported in previous literatures [39].

Performances of the as-prepared MGH in battery were further studied by using a galvanostatic discharge/charge technique. Fig. 5a shows the 1^{st} to 200^{th} cycle discharge/charge curves of the hybrid at a current density of 500 mA g^{-1} in a voltage window of 0.01-3.0 V (vs. Li^+/Li). The initial discharge capacity of the hybrid anode is 1550 mAh g^{-1}, whereas the corresponding reversible charge capacity is 949 mAh g^{-1}, which delivers an initial Coulombic efficiency of 61.2%. The irreversible capacity loss in the 1^{st} cycle is attributed to the electrolyte decomposition and the inevitable formation of solid electrolyte interface (SEI) film on the surface of electrode. During the 2^{nd} cycle, the discharge capacity decreases to 980 $mAhg^{-1}$ with a corresponding charge capacity of 947 mAh g^{-1}, showing a much higher Coulombic efficiency than the 1^{st} cycle. Fig. 5b shows cycling performance of MnO_2 nanowire, rGO and MnO_2/rGO mixture and MGH at a current density of 500 mAg^{-1}. The capacity of the hybrid is gradual decreasing in the first 35 cycles, and then shows an increasing trend. After 200 discharge/charge cycles, the hybrid anode shows a high reversible capacity of 1079 mAh g^{-1}, close to the theoretical capacity of the MnO_2. This capacity value is also much higher than those of the control battery using a pure MnO_2 nanowire anode (197 $mAhg^{-1}$ after 200 cycles), rGO (214 $mAhg^{-1}$ after 200 cycles) and MnO_2/rGO

mixture (416 $mAhg^{-1}$ after 200 cycles). Interestingly, the increasing trend of the capacity of the hybrid is probably due to the reversible growth of the polymeric gel-like film by the kinetically activated electrolyte degradation, which has also been observed in previous literatures [40, 41]. The good cycling performance might be ascribed to the efficient integration of the MnO_2 nanowire with the elastic rGO, which can effectively accommodate the physical strains caused by the large volume changes during the lithiation/delithiation process.

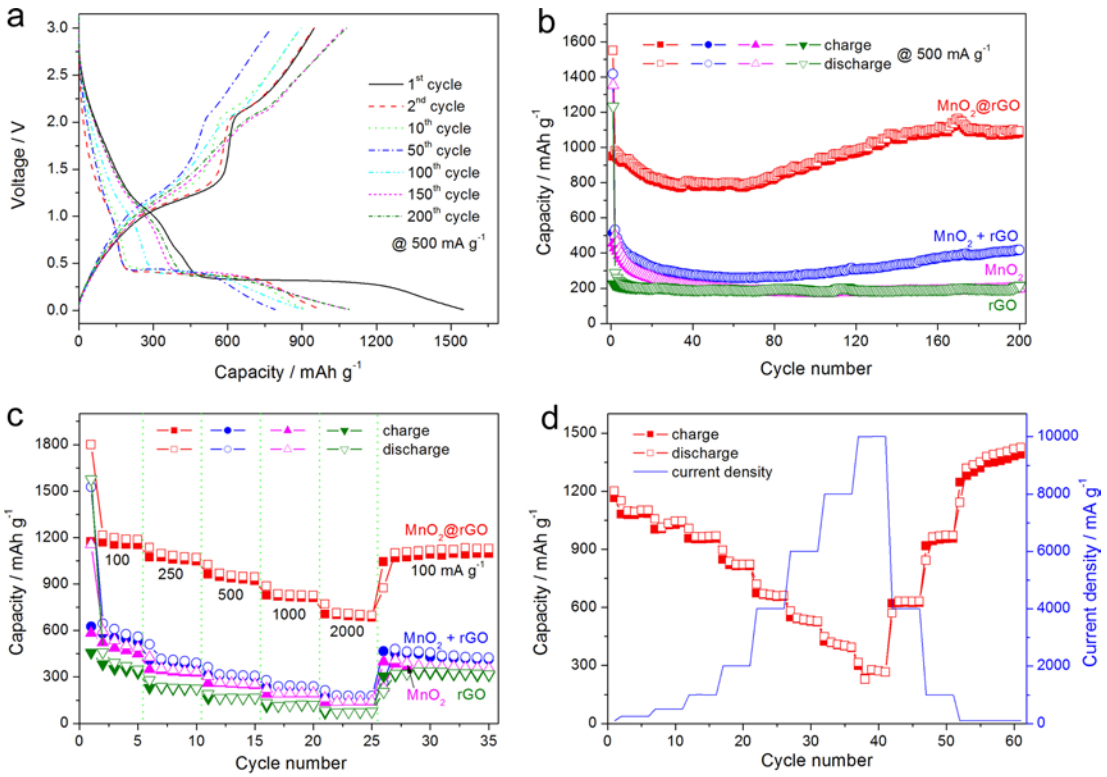

Fig. 5 (a) Discharge and charge voltage profiles and (b) Cycling performance of the MGH at a current density of 500 mA g^{-1}; (c) Rate-capability performance of the pure MnO_2, rGO, MnO_2 nanowires/rGO mixture and MGH at various current densities of 100, 250, 500, 1000, and 2000 mA g^{-1}; (d) Rate-capability test of the MGH from 100 to 10000 mA g^{-1}.

Good rate performances are desirable for developing LIBs with high power densities. The rate capabilities of the as-prepared samples were evaluated at various current densities. As shown in Fig. 5c, the prepared hybrid exhibits the reversible capacities of 1173, 1073, 963, 826, and 705 $mAhg^{-1}$ at the current densities of 100, 250, 500, 1000, and 2000 mA g^{-1}, respectively. Moreover, after changing the current density from 2000 mA g^{-1} to 100 mA g^{-1}, the reversible capacity returns to 1097 mAh g^{-1} after another 10 discharge/charge cycles, showing a good rate capacity and structure stability of the hybrid. Clearly, the rate performance of the hybrid is much better than those of the MnO_2 nanowire, rGO and MnO_2/rGO mixture anode materials. Moreover, even at a high current density of 10000 mA g^{-1}, the reversible capacity can reach 272 mAh g^{-1}, indicating an excellent rate capability of the hybrid (Fig. 5d).

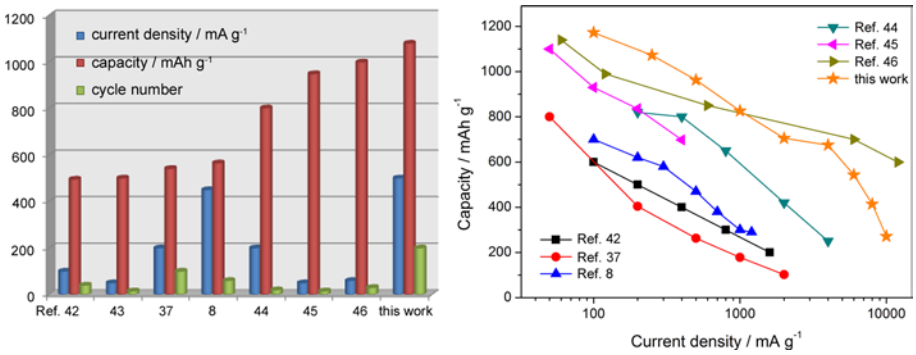

Fig. 6 Comparison on electrochemical properties of MnO_2-carbon hybrids as anode materials for LIB: (a) cycle stability; (b) rate capability.

As shown in Fig. 6, the electrochemical performance of MGH is comparable or better than previously works on MnO_2-carbon hybrids. The good cycle stability and rate capability can be explained by following reasons. The rGO shells provide effective protection against the volume changes of MnO_2 nanowires during

electrochemical processes, while the interconnected conductive networks serve as electron transfer pathway for fast electron transport in the hybrid material, act to reinforce the core-shell structure of MGH and thus enhance the electrical conductivity of the overall electrode.

4. Conclusions

In summary, we reported an efficient solution based method for the fabrication of MGH as LIB anodes. As a result, high capacity, good rate capability and excellent cycling performance are achieved. The enhanced electrochemical performance can be attributed to the advantages of the unique structure, which can effectively alleviate the volume expansion, and facilitate the electron and ion transport. The approach described in this paper may have potential applications in LIB and other energy storage devices.

Acknowledgements

We thank the National Natural Science Foundation of China (Grant Nos. 51075384 and 51205385) and the ‘‘Funds for Distinguished Young Scientists of Gansu Province’’ scheme for financial support.

References

[1] B. Dunn, H. Kamath and J. M. Tarascon, *Science*, 2011, **334**, 928-935.

[2] M. Armand and J. M. Tarascon, *Nature*, 2008, **451**, 652-657.

[3] M. V. Reddy, G. V. S. Rao and B. V. R. Chowdari, *Chem. Rev.*, 2013, **113**,

5364-5457.

[4] Y. H. Dai, H. Jiang, Y. J. Hu and C. Z. Li, *RSC Adv.*, 2013, **3**, 19778-19781.

[5] T. Y. Wei, C. H. Chen, H. C. Chien, S. Y. Lu and C. C. Hu, *Adv. Mater.*, 2010, **22**, 347-351.

[6] J. X. Zhu, Z. Y. Yin, D. Yang, T. Sun, H. Yu, H. E. Hoster, H. H. Hng, H. Zhang and Q. Y. Yan, *Energy Environ. Sci.*, 2013, **6**, 987-993.

[7] Z. S. Wu, W. C. Ren, L. Wen, L. B. Gao, J. P. Zhao, Z. P. Chen, G. M. Zhou, F. Li and H. M. Cheng, *ACS Nano*, 2010, **4**, 3187-3194.

[8] H. Lai, J. X. Li, Z. G. Chen and Z. G. Huang, *ACS Appl. Mater. Interfaces*, 2012, **4**, 2325-2328.

[9] L. Li, A. R. O. Raji and J. M. Tour, *Adv. Mater.*, 2013, **25**, 6298-6302.

[10] X. P. Fang, X. Lu, X. W. Guo, Y. Mao, Y. S. Hu, J. Z. Wang, Z. X. Wang, F. Wu, H. K. Liu and L. Q. Chen, *Electrochem. Commun.*, 2010, **12**, 1520-1523.

[11] G. Yu, L. Hu, M. Vosgueritchian, H. Wang, X. Xie, J. R. McDonough, X. Cui, Y. Cui and Z. Bao, *Nano Lett.*, 2011, **11**, 2905-2911.

[12] P. Poizot, S. Laruelle, S. Grugeon, L. Dupont and J. M. Tarascon, *Nature*, 2000, **407**, 496-499.

[13] X. W. Lou, L. A. Archer and Z. C. Yang, *Adv. Mater.*, 2008, **20**, 3987-4019.

[14] C. He, S. Wu, N. Zhao, C. Shi, E. Liu and J. Li, *ACS Nano*, 2013, **7**, 4459-4469.

[15] Z. C. Yang, J. G. Shen and L. A. Archer, *J. Mater. Chem.*, 2011, **21**, 11092-11097.

[16] W. M. Zhang, X. L. Wu, J. S. Hu, Y. G. Guo and L. J. Wan, *Adv. Funct. Mater.*, 2008, **18**, 3941-3946.

[17] L. Fei, Q. Lin, B. Yuan, G. Chen, P. Xie, Y. Li, Y. Xu, S. Deng, S. Smirnov and H. Luo, *ACS Appl. Mater. Interfaces*, 2013, **5**, 5330-5335.

[18] B. Luo, B. Wang, M. Liang, J. Ning, X. Li and L. Zhi, *Adv. Mater.*, 2012, **24**, 1405-1409.

[19] D. Wang, J. Yang, X. Li, D. Geng, R. Li, M. Cai, T.-K. Sham and X. Sun, *Energy Environ. Sci.*, 2013, **6**, 2900-2906.

[20] S. M. Paek, E. Yoo and I. Honma, *Nano Lett.*, 2009, **9**, 72-75.

[21] J. Lin, Z. Peng, C. Xiang, G. Ruan, Z. Yan, D. Natelson and J. M. Tour, *ACS Nano*, 2013, **7**, 6001-6006.

[22] C. Xu, J. Sun and L. Gao, *J. Mater. Chem.*, 2012, **22**, 975-979.

[23] X. Yang, K. Fan, Y. Zhu, J. Shen, X. Jiang, P. Zhao and C. Li, *J. Mater. Chem.*, 2012, **22**, 17278-17283.

[24] G. Zhou, D.-W. Wang, F. Li, L. Zhang, N. Li, Z.-S. Wu, L. Wen, G. Q. (Max) Lu and H.-M. Cheng, *Chem. Mater.*, 2010, **22**, 5306-5313.

[25] J.-Z. Wang, C. Zhong, D. Wexler, N. H. Idris, Z.-X. Wang, L.-Q. Chen and H.-K. Liu, *Chem. Eur. J.*, 2011, **17**, 661-667.

[26] H. Wang, L.-F. Cui, Y. Yang, H. S. Casalongue, J. T. Robinson, Y. Liang, Y. Cui and H. Dai, *J. Am. Chem. Soc.*, 2010, **132**, 13978-13980.

[27] S. A. Ju, K. Kim, J. -H. Kim and S. -S. Lee, *ACS Appl. Mater. Interfaces*, 2011, **3**, 2904-2911.

[28] S. Yang, X. Feng, S. Ivanovici and K. Müllen, *Angew Chem. Int. Ed.*, 2010, **49**, 8408-8411.

[29] J. He, D. Wu, Z. Gao, F. Xu, S. Jiang, S. Zhang, K. Cao, Y. Guo and K. Jiang, *RSC Adv.*, 2014, **4**, 2068-2072.

[30] S. Zhou, H. Zhang, Q. Zhao, X. Wang, J. Li and F. Wang, *Carbon*, 2013, **2**, 440-450.

[31] Z. Zheng, Y. Cheng, X. Yan, R. Wang and P. Zhang, *J. Mater. Chem. A*, 2014, **2**, 149-154.

[32] X. Wang and Y. Li, *Chem. Eur. J.*, 2003, **9**, 300-306.

[33] F. Kim, L. J. Cote and J. Huang, *Adv. Mater.*, 2010, **22**, 1954-1958.

[34] D. Li, M. B. Muller, S. Gilje, R. B. Kaner and G. G. Wallace, *Nat. Nanotechnol.*, 2008, **3**, 101-105.

[35] M. S. Wu and P. C. J. Chiang, *Electrochem. Commun.*, 2006, **8**, 383-388.

[36] M. S. Wu, P. C. J. Chiang, J. T. Lee and J. C. Lin, *J. Phys. Chem. B*, 2005, **109**, 23279-23284.

[37] Y. Wang, Z. J. Han, S. F. Yu, R. R. Song, H. H. Song, K. Ostrikov and H. Y. Yang, *Carbon*, 2013, **64**, 230-236.

[38] B. Sun, Z. Chen, H.-S. Kim, H. Ahn and G. Wang, *J. Power Sources*, 2011, **196**, 3346-3349.

[39] M. Kundu, C. C. A. Ng, D. Y. Petrovykh and L. Liu, *Chem. Commun.*, 2013, **49**, 8459-8461.

[40] G. M. Zhou, D. W. Wang, F. Li, L. L. Zhang, N. Li, Z. S. Wu, L. Wen, G. Q. Lu and H. M. Cheng, *Chem. Mater.*, 2010, **22**, 5306-5313.

[41] W. Wei, S. Yang, H. Zhou, I. Lieberwirth, X. Feng and K. Müllen, *Adv. Mater.*,

2013, **25**, 2909-2914.

[42] A. Yu, H. W. Park, A. Davies, D. C. Higgins, Z. Chen and X. Xiao, *J. Phys. Chem. Lett.*, 2011, **2**, 1855-1860.

[43] A. L. M. Reddy, M. M. Shaijumon, S. R. Gowda and P. M. Ajayan, *Nano Lett.*, 2009, **9**, 1002-1006.

[44] H. Xia, M. Lai and L. Lu, *J. Mater. Chem.*, 2010, **20**, 6896-6902.

[45] C. X. Guo, M. Wang, T. Chen, X. W. Lou and C. M. Li, *Adv. Energy Mater.*, 2011, **1**, 736-741.

[46] Y. Zhang, H. Liu, Z. Zhu, K. Wong, R. Mi, J. Mei and W. Lau, *Electrochim. Acta*, 2013, **108**, 465-471.

Figure captions:

Scheme 1 Fabrication process of MGH.

Fig. 1 XRD patterns of MnO_2 and MGH.

Fig. 2 (a) AFM morphological image and a corresponding cross-section analysis of the as-prepared rGO; b, c) FESEM images of MnO_2 nanowires and MGH.

Fig. 3 (a, b) TEM and (c, d) HRTEM images of the MGH. Fig. d is the enlarged HRTEM image of the outlined area in Fig. c.

Fig. 4 (a) CV curves of the MGH at a scan rate of 0.1 mV s^{-1}; (b) Discharge and charge voltage profiles of the MGH at a current density of 100 mA g^{-1}.

Fig. 5 (a) Discharge and charge voltage profiles and (b) Cycling performance of the MGH at a current density of 500 mA g^{-1}; (c) Rate-capability performance of the pure MnO_2, rGO, MnO_2 nanowires/rGO mixture and MGH at various current densities of 100, 250, 500, 1000, and 2000 mA g^{-1}; (d) Rate-capability test of the MGH from 100 to 10000 mA g^{-1}.

Fig. 6 Comparison on electrochemical properties of MnO_2-carbon hybrids as anode materials for LIB: (a) cycle stability; (b) rate capability.

Assembly of MnO_2 nanowires@reduced graphene oxide hybrid with interconnected structure for high performance lithium ion battery

Zhangpeng Li[ab], Jinqing Wang*[a], Zhaofeng Wang[a], Yongbing Tang[b], Chun-Sing Lee*[b], Shengrong Yang[a]

[a] State Key Laboratory of Solid Lubrication, Lanzhou Institute of Chemical Physics, Chinese Academy of Sciences, Lanzhou 730000, P. R. China

[b] Center of Super-Diamond and Advanced Films (COSDAF), Department of Physics and Materials Science, City University of Hong Kong, Kowloon, Hong Kong SAR, P. R. China

Corresponding authors. Tel.: +86-931-4968076 (J. Wang); +852-34427826 (C. Lee)

E-mail addresses: jqwang@licp.cas.cn (J. Wang); apcslee@cityu.edu.hk (C. Lee)

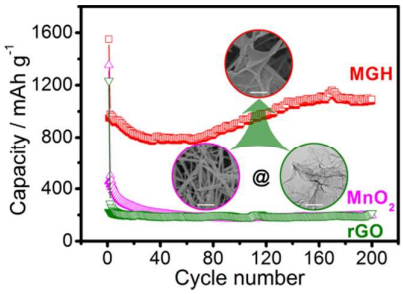

MnO_2 nanowires@rGO hybrid delivers a high reversible capacity of 1079 mAh g^{-1} over 200 cycles at a current density of 500 mA g^{-1}, and excellent rate capability.